Highly active screen-printed Ir-Ti_4O_7 anodes for proton exchange membrane electrolyzers.

Tiago Lagarteira[a,b], Feng Han[a]*, Tobias Morawietz[c], Renate Hiesgen[c], Daniel Garcia Sanchez[a], Adélio Mendes[b], Aldo Gago[a]*, Rémi Costa[a]*

[a] Institute of Engineering Thermodynamics, German Aerospace Center, Pfaffenwaldring 38-40, Stuttgart, Germany

[b] present address: Laboratory for Process Engineering, Environmental, Biotechnology and Energy (LEPABE), Faculty of Engineering of University of Porto, Rua Roberto Frias s/n, 4200-465 Porto, Portugal

[c] University of Applied Sciences Esslingen, Dep. of Basic Science, Kanalstrasse 33, Esslingen, Germany

*Corresponding authors

E-mail addresses:

feng.han@dlr.de; aldo.gago@dlr.de; remi.costa@dlr.de

Keywords

Proton exchange membrane water electrolysis; Membrane electrodes assembly; Catalyst coated membrane; Iridium loading; Ceramic support; Screen printing.

Abstract

Electroceramic support materials can help reducing the noble-metal loading of iridium in the membrane electrodes assembly (MEA) of proton exchange membrane (PEM) electrolyzers. Highly active anodes containing Ir-black catalyst and submicronic Ti_4O_7 are manufactured through screen printing technique. Several vehicle solvents, including

ethane-1,2-diol; propane-1,2-diol and cyclohexanol are investigated. Suitable functional anodic layer with iridium loading as low as 0.4 mg cm^{-2} is obtained. Surface properties of the deposited layers are investigated by atomic force microscopy (AFM). The most homogeneous coating with the highest electronic conductivity is obtained using cyclohexanol. Tests in PEM electrolyzer operating at 1.7 V and 40 °C demonstrate that the CCM with anode coated with cyclohexanol presents a 1.5-fold higher Ir-mass activity than that of the commercial CCM.

1. Introduction

Intermittency and fluctuation of renewable energy sources remain major issues for an efficient utilization, while the power flow and utility frequency of the grid need to be steadily regulated and balanced. Hydrogen can be produced through water electrolysis with the surplus from renewables when available and stored as a carbon neutral energy carrier. Proton exchange membrane (PEM) water electrolysis is a promising technology for coupling renewables with hydrogen due to the wide operating range and the fast response [1–3]. In particular, the compact system design, high efficiency and easy maintenance are advantageous features comparing to the mature alkaline electrolysis technology [1,4,5]. Yet, the penetration of PEM electrolyzer systems at the megawatt scale will be hindered by the high cost and scarcity of catalyst materials, together with the manufacturing of the membrane electrodes assembly (MEA), which currently represent approximately 20 % of the overall costs of the PEM electrolyzer stack [6]. Therefore, there is a potential for cost reduction by decreasing the used amount of precious group metals (PGM) and optimizing the catalyst coating process in the production of MEAs.

A reduction in the catalyst loadings is not only important due to high price of the precious metals but also the scarcity of platinum and mainly iridium [7]. Despite some

recent advances that took several years of research [8,9], the state-of-the-art anode still demands high iridium loadings of *ca.* 2-4 mg cm^{-2} [10,11], to balance the sluggish kinetics and the high charge transfer overpotential caused by the oxygen evolution reaction (OER). Ceramic supports like Magnéli-phase titanium sub-oxides (TiO_2, Ti_4O_7 and Ti_5O_9) are promising catalyst supports, providing a higher catalytic stability and resistance to corrosion in the harsh environment of the electrolyzer anode in comparison to the typical carbon-based supports used in PEM fuel cells [12–20].

For the manufacturing, screen printing is a widespread and common cost-efficient printing technique that can be used to produce catalyst coated membranes (CCM-MEA), where the catalysts are directly deposited on a proton exchange membrane – typically Nafion. Some reports on the fabrication of MEAs for PEM fuel cells with screen printing are available. But in most of them, the catalyst deposition is carried out on the gas diffusion layer (GDL) or on PTFE sheets with posterior decal transfer to the membrane. This is the usual strategy to avoid typical processing issues like membrane swelling when it contacts with organic solvents [21–24]. The overcome of the swelling issue is a key challenge as direct catalyst deposition on the membrane may provide better contact between the catalyst layer and the electrolyte thus reducing interfacial contact resistances. Kim and co-workers proposed a treatment [25] in which the membrane was exchanged from the H^+ form to Na^+ form before coating. The protonic reconversion was performed after the catalyst layer was deposited and dried. Nonetheless, no report is found in the literature of screen-printed catalyst layers directly on the membrane for PEM electrolyzers [11].

Composition of the catalyst ink affects not only the coating process itself - by governing the rheological properties - but also affects the microstructure of the coated layer. The properties of the catalyst ink should be optimized not only for the coating process but

also for maximizing the connection of catalytic sites to both electronic and ionic conductive phases, thus ensuring the overall performance of the electrolyzer. The idea of using solubilized Nafion ionomer in catalyst inks or suspensions has been widely accepted for extending protonic vehicular conduction inside 3D-structures of the catalyst layers [26–28]. More recently, Chan and Eikerling reported that ionomer-free ultra-thin catalyst layers (20 - 500 nm thick) rely entirely on liquid water for proton conduction [29]. Therefore, a fully humidified catalyst layer would be beneficial, enabling proton conduction exclusively by the Grotthuss mechanism [30]. In the case of screen-printed catalyst layers, with thickness in the micrometer range, ionomer distribution and its orientation should be tuned for connecting the most active sites to the protonic conductive phase while not hindering electronic conductivity of the catalyst support and mass diffusion in the porous structure of the catalyst layer [31].

In this work, highly-active anodes with inexpensive catalyst support and low catalyst loading were fabricated via a cost-effective and scalable screen printing technique. Moreover, the properties of the developed layers were characterized and investigated through diagnostic tools such as TGA, AFM and electrochemical single cell tests.

2. Experimental

2.1 CCM fabrication

2.1.1 Screen printing of the anode

In the preparation of the screen printing inks, summarized in Table 1, 30 wt% Iridium Black (Umicore) was mixed with 70 wt% Ti_4O_7 catalyst support (Changsha Purong Chemical Engineering Inc.) using a mortar and a pestle. Ethane-1,2-diol (Sigma Aldrich), propane-1,2-diol (VWR) and cyclohexanol (VWR) were used as organic solvents for the inks (physicochemical properties shown in Table 2). The ratio between

Nafion ionomer and the total solid particles was kept at 30 wt% [32]. The solvents from a 20 wt% Nafion solution (Sigma Aldrich) were evaporated during the mixing and, only then, the chosen organic solvent was added. The solid content in the screen printing inks was kept at 37.5 wt%, except for the ink used in the effectiveness assessment of the membrane swelling treatment which contained a lower (but not determined) weight ratio of solid particles.

Ink formulations	**Catalyst (7.875 wt%)**	**Catalyst support (18.375 wt%)**	**Binder (11.25 wt%)**	**Solvent (62.5 wt%)**
A	Ir Black	Ti_4O_7	Nafion ionomer	Ethane-1,2-diol
B	Ir Black	Ti_4O_7	Nafion ionomer	Propane-1,2-diol
C	Ir Black	Ti_4O_7	Nafion ionomer	Cyclohexanol

Table 1 - Screen printing ink formulations; weight ratios based on the total weight of the ink.

Solvent	**Viscosity * 10^{-3} (Pa s) @ 298 K**	**Vapor pressure (Pa) @ 293 K**	**Relative permittivity (ε)**	**Boiling temperature (K @ 10^5 Pa)**
Ethane-1,2-diol	16.13	8	37 @ 298 K	470.75
Propane-1,2-diol	42.00	17.3	32 @ 293 K	461.35
Cyclohexanol	54.60	133.3	15 @ 293 K	434.15

Table 2 - Physical properties of organic solvents used in screen printing inks.

Nafion 212 membrane was cut into squares with a size 7 cm x 7 cm and, after removing the protection foils and conditioning at ambient humidity, they were weighted. Subsequently, they were placed on a porous metal substrate, enabling the use of a vacuum positioning and fixing system during the coating process. An Aurel 900 screen printer equipped with a Koenen Typ-10 M6 mesh (4 cm^2 of open area) was used for

coating the anodes of the CCMs. The printing pressure was set to 1.5 N cm^{-2} and the distance between the screen and the substrate was 0.8 mm.

After coating, the samples were dried firstly on the screen printing holder for 10 minutes under infrared radiation produced by an incandescent lamp (40 W, distance 10 cm) to remove most of the solvent, and then dried at 348 K for 30 minutes in a drying oven. After conditioning at ambient humidity, the one-side coated membranes were again weighted for catalyst loading calculation purposes. The iridium loading was calculated based on weight difference of the membranes before and after the anode coating, and confirmed by thermal gravimetric analysis (TGA).

2.1.2 Wet spraying of the cathode

Since the focus of this work was the anode processing, the cathode was deposited by the state-of-the-art and widely used wet spray coating method. Thus, the differences in performance could be only related to the screen printing parameters. This technique was selected for processing the platinum-based cathodes since it allows achieving high performances with good reproducibility [33–35]. The spraying suspension was prepared by mixing 60 wt% Pt/C (Johnson Matthey) with 50 vol% water in isopropanol, considering the solvents from a 5 wt% Nafion solution (Ion Power). First, HPLC purity grade water was added the catalyst powder to avoid nanoparticles ignition when in contact with low molecular alcohols. Nafion ionomer content was kept at 35 wt% relatively to the solids in the spraying suspension. The total solid content in the suspension was 0.8 wt%. A heated vacuum table at 378 K was used during the wet spray deposition to dry the suspension solvents and simultaneously avoiding membrane swelling. After the cathode was coated, the CCM was hot pressed at 1.75 MPa and 398 K for 5 minutes.

2.1.3 Membrane swelling treatment

A membrane treatment reported by Kim and co-workers [24,25,36] was used to avoid swelling of the Nafion membrane caused by ethane-1,2-diol. In short, the membrane was boiled in an aqueous solution of 0.25 M NaOH for 15 minutes. After exchanging from protonic to sodium ionic form, the membrane was washed and boiled in deionized water for 10 minutes before being screen-printed. Following, the membrane was coated, dried and hot pressed to produce the CCM. Finally, the CCM was boiled in an aqueous solution of H_2SO_4 (0.5 M) for 30 minutes for reprotonation. The CCM was then rinsed three times one minute each in deionized water to remove any remaining acid traces before testing. The iridium loading of the two anodes used for assessing the effectiveness of the membrane swelling treatment were equal, however they were not calculated.

2.2 Thermal gravimetric analysis (TGA)

The anode-coated membrane with the ink using propane-1,2-diol as solvent was cut in circular samples of 5 mm in diameter for the TGA measurement. The analysis was performed using a thermal gravimetric analyzer (NETZSCH STA 449 C) and a DSC/TG pan Pt under air atmosphere, heated from 303 K to 1073 K at 5 K min^{-1}.

2.3 Atomic force microscopy (AFM)

The local properties of the surface were investigated by atomic force microscopy (AFM). For the AFM measurements performed with a Multimode 8 AFM (Bruker, Karlsruhe), a piece of the MEA was cut out of the center with a razorblade. The CCM sample was glued with conductive adhesive tape onto a steel disc with the anode facing to the top. The anode was additionally connected with silver paste to ensure a low electrical resistance. Platinum/iridium coated AFM tips (PPP-NCHPt), with a nominal

spring constant of 42 N m^{-1}, were used in conductive tapping mode (PF-TUNA, Bruker). In PF-TUNA mode, a force distance curve is evaluated at every image point to reveal adhesion, stiffness and deformation. A built-in lock-in amplifier averaged the simultaneously measured current. Images with a length scale of 5 µm and 512 x 512 pixel were recorded at a scan rate of 0.5 Hz. The relative humidity during measurements was 30 ± 5 %. Evaluation of the porosity was performed with the bearing analysis tool of the Bruker nanoscope analysis software. For each anode, three 25 μm^2 measurements were performed. For the porosity determination, the 25 μm^2-sized measurements were evaluated at 4 areas of 6.25 µm side length. For the conductive area evaluation, the threshold was set to 0.1 nA and the applied voltage was 2 V. The threshold for the adhesion force and deformation evaluation was derived by profile lines across high and low value areas. The adhesion force/deformation values determined by the turning points were used as threshold values, respectively.

2.4 Single cell measurements

The investigation of the dynamic response of the developed CCMs was performed on home-made single cell PEM electrolyzer test rig with an electrode area of 4 cm^2 [37]. The cell temperature was maintained at 313 K and it was fed with HPLC purity grade water. A potentiostat/galvanostat equipped with an electrochemical impedance spectroscopy (EIS) module (Zahner Instruments) was used to evaluate the performance of the electrolyzer in a single-cell configuration.

Ti-coated stainless steel bipolar plates by vacuum plasma spraying [38–40] without flow field were used for the cell assembly. At the anode side, a Ti mesh was put between the bipolar plate and a sintered porous titanium layer (PTL) current collector of *ca*. 1 mm thickness, > 40% porosity coated with Pt-IrOx (Magneto Special Anodes B.V.). At the cathode side, three carbon papers (Toray paper 030) were used as gas

diffusion layer (GDL) to prevent the destruction of the carbon paper upon the pressure increase caused by the evolution of H_2. A protocol of measurements was defined using mild conditions for electrolyzer operation to avoid a possible fast degradation of the produced CCMs. The evolution of the current density was measured at 1.7 V in potentiostatic conditions. EIS was performed at 35 mA cm^{-2} to enable a stable recording using a small perturbation of 5 mV. The parameters of the EIS spectra were fitted with an equivalent circuit [41] with (RQ) elements, representing a parallel combination of resistance and pseudo-capacitance for each catalyst layer. The fitted parameters are displayed in Table 3. R_S corresponds to the HFR in which the major contribution is assigned to the electrolyte. R_1 and R_2 are associated to charge transfer resistances of HER and OER, respectively. The onset of mass diffusion effects was not included in the fittings. A previously activated commercial CCM (E300 from Greenerity), containing 2.25 mg cm^{-2} of iridium at the anode, 1.25 mg cm^{-2} of platinum at the cathode and Nafion 212 membrane, was also tested under the same cell configuration for comparison purposes.

3. Results and discussion

3.1 The role of solvents and membrane swelling treatment

Figure 1 shows the anode-coated membranes, after being screen-printed and dried. The red circles point out the membrane swelling spots. The thickness of the anodes was *ca.* 13 µm. The ink using cyclohexanol was the only one that did not generate any visible membrane swelling. The ink using ethane-1,2-diol generated more membrane swelling when compared with the ink using propane-1,2-diol. After hot pressing, swelling spots (red circles) could not be seen in all CCMs. However, only the sample using

cyclohexanol presented uniform coating which could guaranty homogeneous catalyst loading.

The generation of swelling is related to the affinity between hydroxyl groups of the solvents and sulfonated groups of Nafion. Cyclohexanol has just one hydroxyl group and a heavier closed carbon chain while propane-1,2-diol and ethane-1,2-diol have two hydroxyl groups. A heavier carbon chain decreases the polarity of the molecule thus decreasing its interaction with sulfonated groups of Nafion.

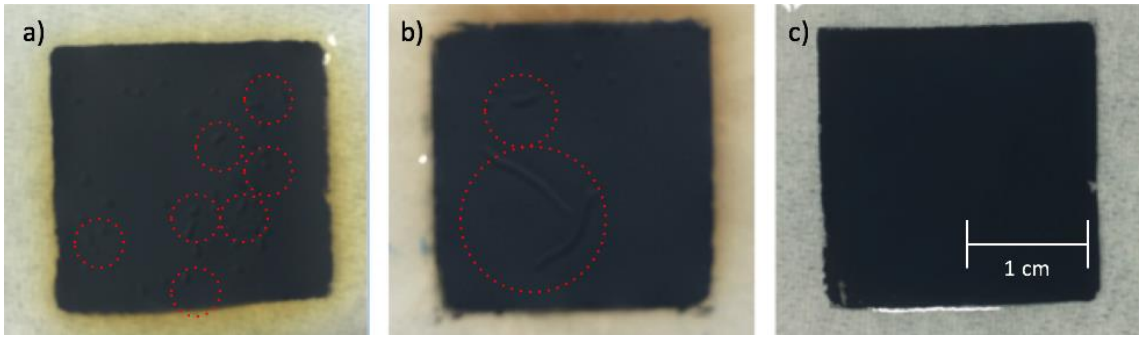

Figure 1: Images of the anodes, before hot press, coated using different solvents: a) ethane-1,2-diol; b) propane-1,2-diol; c) cyclohexanol.

The membrane treatment procedure proposed by Kim et al. [25], proved to be effective for minimizing membrane swelling. Figure 2a shows the chronoamperometries at 1.7 V of two CCMs with anode coated with ethane-1,2-diol as solvent of the screen printing ink. The replacement of protons by heavier Na^+ reduced the affinity between Nafion sulfonated groups and ethane-1,2-diol. A larger cation ($Na^+ > H^+$) not only limits the free space for sulfonated groups to move, but also disables those sites for hydrogen-type bonds with the solvent hydroxyl groups. The two curves display different starting points and slopes before steady-state behavior, but the electrochemical activity of both CCMs equalizes for longer times. At the end of tests, the swelling treated CCM slightly outperformed the CCM without treatment, indicating that the ionic form modification

and posterior reprotonation does not hinder the electrochemical performance of the CCM.

Figure 2b presents the impedance spectra (at 35 mA cm^{-2}) of CCMs subjected and not subjected to membrane treatment, recorded at the end of tests. The overall impedance of the electrolyzer with treated CCM is smaller than that with the untreated CCM (difference of *ca.* 800 mΩ cm^2) and the largest contribution for the overall impedance is assigned to charge transfer resistances of OER with values of 2.1 Ω cm^2 and 2.5 Ω cm^2, respectively [41–44]. The high frequency resistance (HFR) is 250 mΩ cm^2 for the treated CCM, that is even lower than that of the untreated CCM - 300 mΩ cm^2. This indicates that the swelling treatment has not a negative effect on the ohmic resistance and on the membrane conductivity.

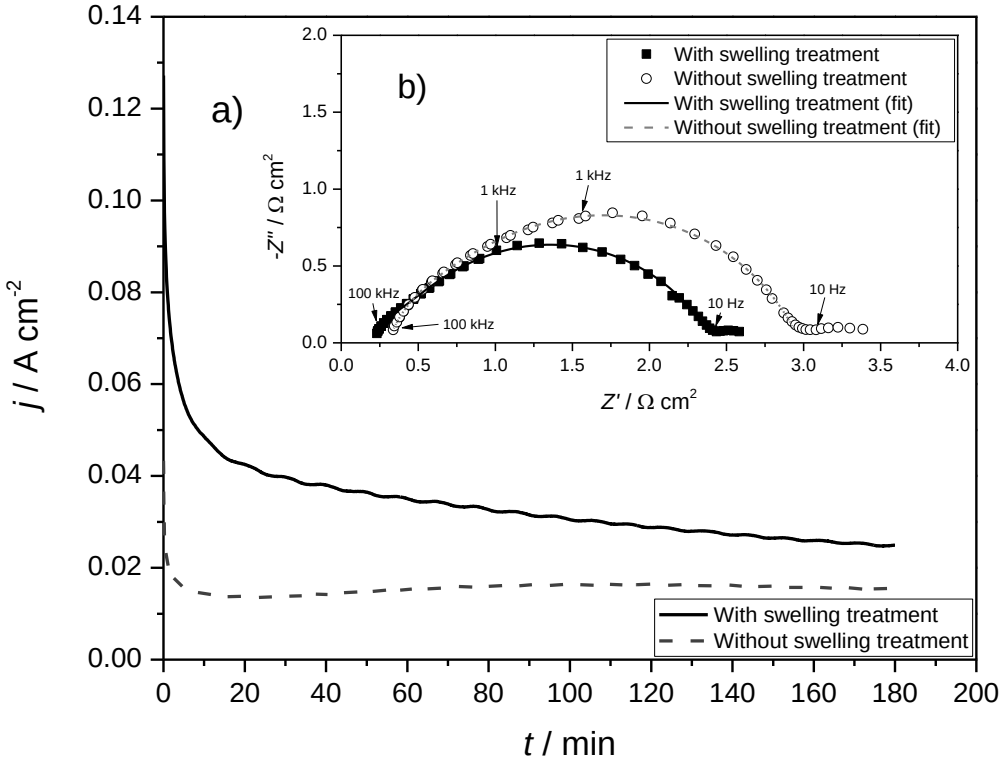

Figure 2: a) Chronoamperometries (at 1.7 V and 40 ºC) of CCMs with and without swelling treatment. b) Impedance spectra (at 35 mA cm^{-2} and 40 ºC) of CCMs with and without swelling treatment.

The influence of the solvents used on the surface structure of the anodes is visible in the AFM topography measurements in Figure 3. In Figure 3a and Figure 3c, prepared using cyclohexanol and using propane-1,2-diol, respectively; more pores are present at the surface when compared to Figure 3b, prepared using ethane-1,2-diol. At this anode, beside a few open pores, regions with a smooth surface are present, and are most-likely Nafion ionomer. The adhesion force and deformation mappings given in Figure 4 reveal the distribution of catalyst and ionomer. Ionomer can be discerned from the catalyst and support particles by its high adhesion (bright areas in Figure 4, a-c), high deformation values (bright areas in Figure 4, d-f), and low DMT modulus (stiffness) - Figure S2 in Supplementary Information [45–47].

The surface porosity of the three 25 μm^2 topography images of the prepared anodes was evaluated. The porosity of the anode prepared using cyclohexanol solvent was the highest of the three samples, 26 ± 2 %, followed by the sample prepared using propane-1,2-diol with 20 ± 2 %. The anode prepared using ethane-1,2-diol had the lowest porosity with 13 ± 2 %. Due to the restriction to horizontal geometry, the AFM-determined porosity values are generally lower than those determined by other methods.

The coatings prepared using cyclohexanol and using propane-1,2-diol as solvents presented a comparably good distribution of ionomer and catalyst particles at the surface, as illustrated in Figure 4. The maximum size of connected ionomer particle area was determined from particle analysis of the adhesion image evaluation. For anodes prepared using cyclohexanol as solvent, the size was the smallest, 1280 ± 170 nm^2; for

anodes prepared using propane-1,2-diol, the size was 1900 ± 240 nm^2; and the largest size was displayed by anodes prepared using ethane-1,2-diol, 3420 ± 40 nm^2. In conclusion, the catalyst particle distribution of the anode surface prepared using ethane-1,2-diol was the least homogeneous.

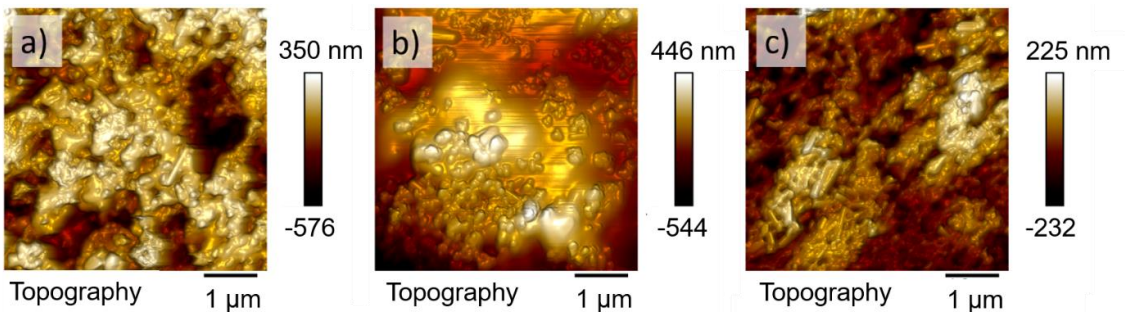

Figure 3: AFM topography images of anodes prepared using different solvents: a) cyclohexanol, b) ethane-1,2-diol, c) propane-1,2-diol.

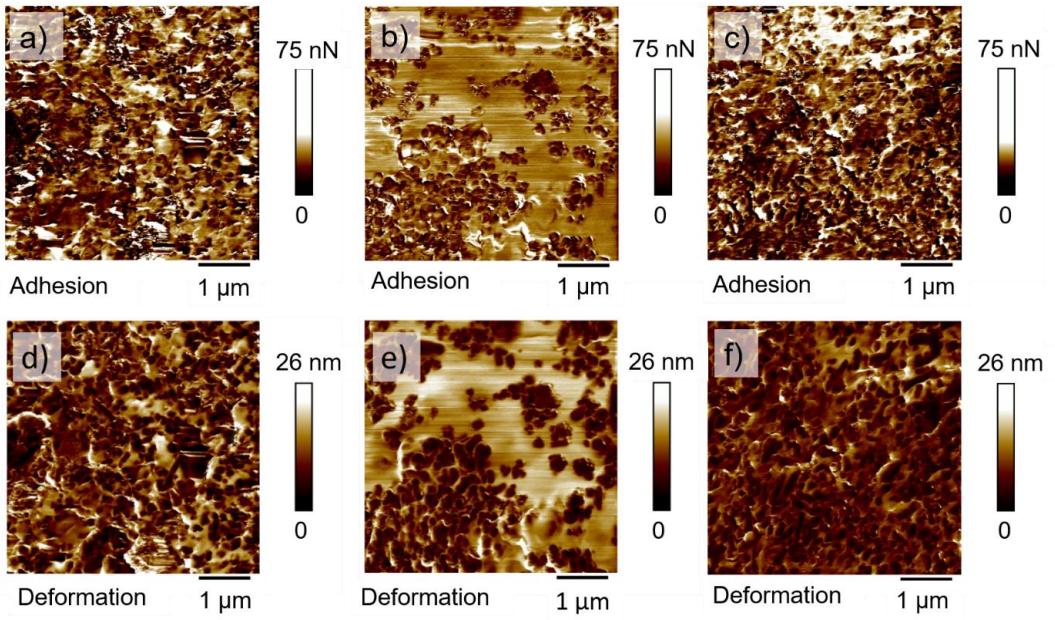

Figure 4: AFM adhesion force measurements at the anodes prepared using different solvents. a) cyclohexanol, b) ethane-1,2-diol, c) propane-1,2-diol. Correlated deformation measurements for the anodes prepared using different solvents: d) cyclohexanol, e) ethane-1,2-diol, f) propane-1,2-diol.

3.2 *Catalyst loading calculation*

The manufactured anodes contained Ir-loadings of 0.4 ± 0.02 mg cm^{-2} according to the differences in the weight of the membrane before and after coating the anodes.

TGA (Figure S1 at Supplementary Information) was performed to the anode coated using propane-1,2-diol for validation of the weight difference calculation. The mass-losses at 400 ºC correspond to the Nafion membrane and ionomer decomposition. These results are in accordance with the work of Deng and co-workers [48] who noted major decomposition between 355°C–560°C corresponding to HF, carbonyl fluorides, and species exhibiting C–F stretching vibrations. In the work by Chen et al. [49], Ti_4O_7 does not show any thermal oxidation below 300 ºC. More recently, Senevirathne and co-workers [50] reported that Ti_4O_7 oxidizes to the more stable TiO_2 at 550 ºC with a weight gain of 6.2 % (higher than the theoretical value of 5.3 %). Iridium nanoparticles oxidize to IrO_2 during the TGA measurements under airflow, which additionally increases the total weight gain.

The remaining mass after the TGA measurement was found to be *ca*. 5.3 % of the initial mass of 4.90 mg. Since the species present after TGA are not Ir and Ti_4O_7, but instead IrO_2 and TiO_2, different oxygen uptake by the two species was considered to calculate IrO_2 mass content at the end of TGA. The original mass fraction of Ir in the mixture of Ir/Ti_4O_7 was 30 wt%. After the TGA, the theoretical mass fraction of IrO_2 in the mixture of IrO_2/TiO2 would be 32.2 wt% (calculation in Supplementary Information). Finally, from the remaining TGA mass (correspondent to IrO_2 and TiO_2) and the area of the TGA sample, one can obtain the Ir-loading of 0.42 mg cm^{-2}.

The cathode of the CCM was sprayed with 100 µl cm^{-2} of catalyst suspension, and estimated Pt loading was 0.5 mg cm^{-2}, assuming 10 % of suspension loss in the gun and borders of the spraying area.

3.3 Electrical surface conductivity

In Figure 5, the fraction of high deformation, high adhesion and non-conductive surface area of the three differently prepared anodes is given. When measuring the ionomer coverage, the highly deformable area fraction is the most significant signal because, by surface deformation values, only regions with approximately more than 30 nm thick ionomer layers at the surface are counted. Due to the high surface sensitivity to the adhesion force, the area measured by adhesion contrast also includes particles covered by a very thin ionomer layer erroneously rated as ionomer. The ionomer area at the surface of the sample prepared using ethane-1,2-diol (42 ± 2 %) was larger than that of the two other samples, which had approximately the same ionomer area fraction of 36 ± 2 % (propane-1,2-diol) and 35 ± 2 % (cyclohexanol). In addition, the non-conductive area derived from the current measurements was much larger in all three cases. The sample prepared using propane-1,2-diol had the largest non-conductive area, followed by the samples prepared using ethane-1,2-diol and cyclohexanol, respectively. This discrepancy can be explained by the different nature of the signals. A conductive surface spot needs to be electrically connected to the back electrode, while the nanomechanical properties reflect the properties of surface and sub-surface. In conclusion, the conductive network was the best for the sample prepared with cyclohexanol, followed by the samples prepared by using ethane-1,2-diol and propane-1,2-diol, respectively.

The AFM-derived conductive area fractions follow the same slope as the current revealed by the polarization measurements of the anodes after a short running period

(Figure 6). Examples of the AFM current measurements are given in Figure 7; a correlation between electronic conductivity and conductive surface area is apparent. Consequently, a decrease of ionomer content could enhance the electrolyzer performance.

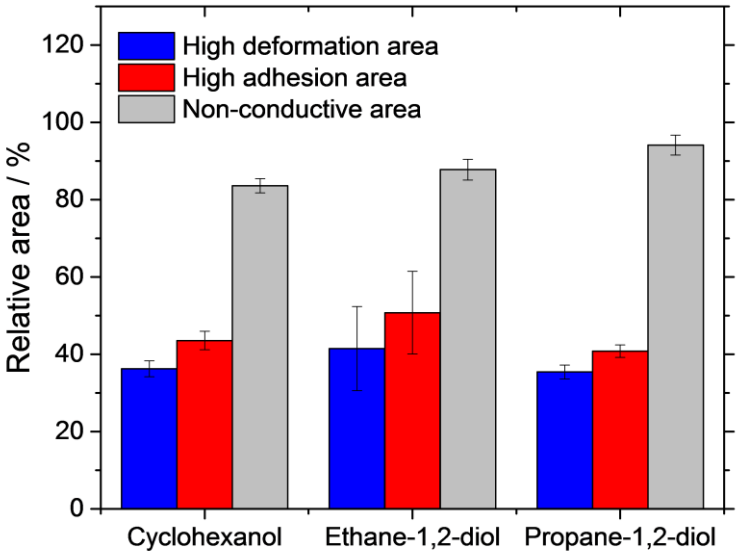

Figure 5: Relative area of adhesion, deformation and non-conductive area at the surfaces of the three anodes prepared using different solvents.

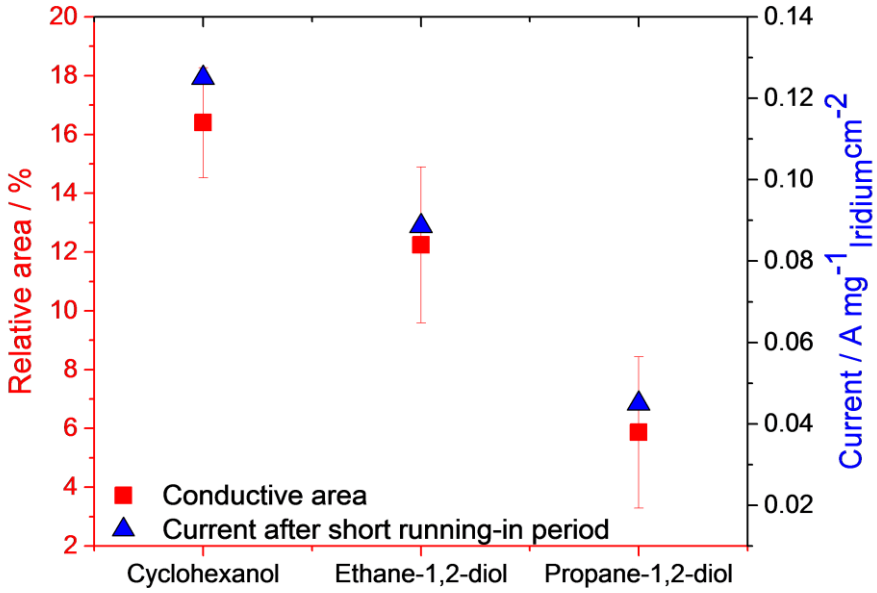

Figure 6: Comparison of AFM-derived conductive area and current after short running-in period for the three differently prepared anodes.

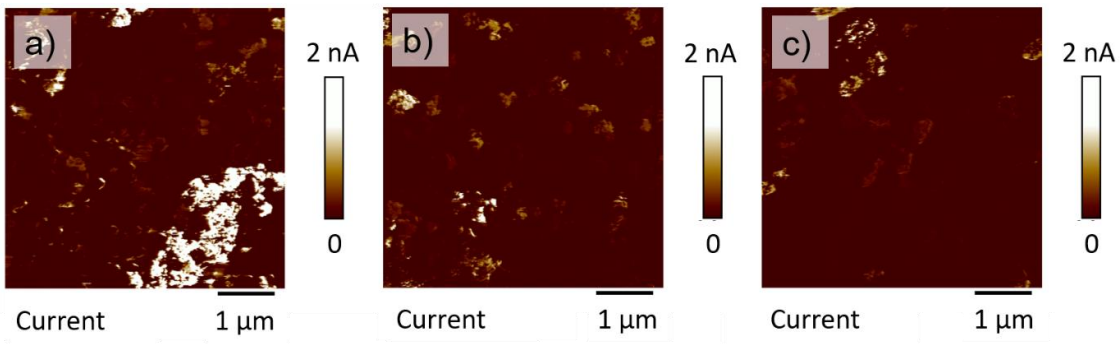

Figure 7: AFM measurements of conductive area for the anodes prepared using different solvents: a) cyclohexanol, b) ethane-1,2-diol, c) propane-1,2-diol.

In Figure 8, the surface topography of 400 µm^2 of the three different surface structures is shown; the roughness was evaluated from the AFM topography images. The highest roughness of 120 ± 30 nm was observed for the anode prepared using ethane-1,2-diol as

solvent, followed by the sample prepared using cyclohexanol - 110 ± 10 nm; the lowest roughness was determined for the sample prepared using propane-1,2-diol, with a roughness of 54 ± 2 nm. The higher roughness of sample prepared using ethane-1,2-diol is likely caused by the large height differences between the ionomer agglomerates and the catalyst-containing phase and does not represent the roughness of the surface film; the large inhomogeneity is also indicated by the large error. The sample prepared using ethane-1,2-diol exhibited the most heterogeneous distribution, with regions of high catalyst density and large ionomer areas without any catalyst.

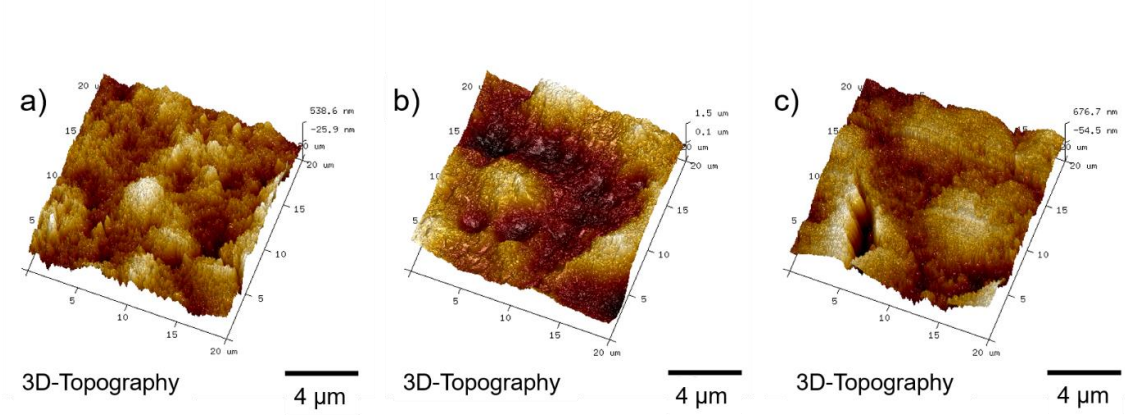

Figure 8: AFM 3D-topography measurements of the anodes prepared using different solvents: a) cyclohexanol, b) ethane-1,2-diol, c) propane-1,2-diol.

3.4 Electrochemical performance

Chronoamperometries of the CCMs with anodes coated using different solvents are depicted in Figure 9a. After 180 min of operation, the anode coated using cyclohexanol solvent delivered the highest current density at 1.7 V, followed by the anode coated using propane-1,2-diol. The relative permittivity of the ink solvents impacts on the ionomer conformation and distribution in the catalyst layer. The three solvents used in this work (with $\varepsilon > 10$) make Nafion ionomer remain in solution form [24]. From Figure

9a, electrochemical activity is higher for solvents with lower relative permittivity. This fact suggests that solvents with ε values closer to the colloidal form frontier ($3 < \varepsilon < 10$) of the ionomer generate a better triple-phase boundary, thus promoting a better catalyst utilization. The single curve with a relatively constant current value at end of tests corresponds to the anode coated using ethane-1,2-diol as ink vehicle. The slow electrochemical activity improvement observed in Figure 9a can be attributed to CCM activation phenomenon, which is a typical procedure in PEM fuel cells [51]. The origin of this improvement might be related to the accommodation of the microstructure of the catalyst layer and membrane/ionomer. Additionally, high potentials typical in water electrolysis (operation above 1.4 V) enable oxidation of Ir to the more OER-active IrO_2 [52]. A commercial CCM (E300 from Greenerity) was also tested under the same conditions (Figure S3 in Supplementary Information). The commercial CCM had been previously activated by the manufacturer. Mass activities of the fabricated CCMs are presented in Figure 9b. Even though the CCMs coated using propane-1,2-diol and cyclohexanol did not reach steady-state activity at end of tests, they already exceeded the iridium-mass activity of E300 at 1.7 V and 40 ºC. The screen-printed CCM using cyclohexanol as ink vehicle delivered the highest Ir-mass activity, that is 0.26 A mg^{-1} at 1.7 V and 40 ºC. Compared to the commercial CCM, a higher catalyst utilization was observed for the screen printed CCM using cyclohexanol as a solvent.

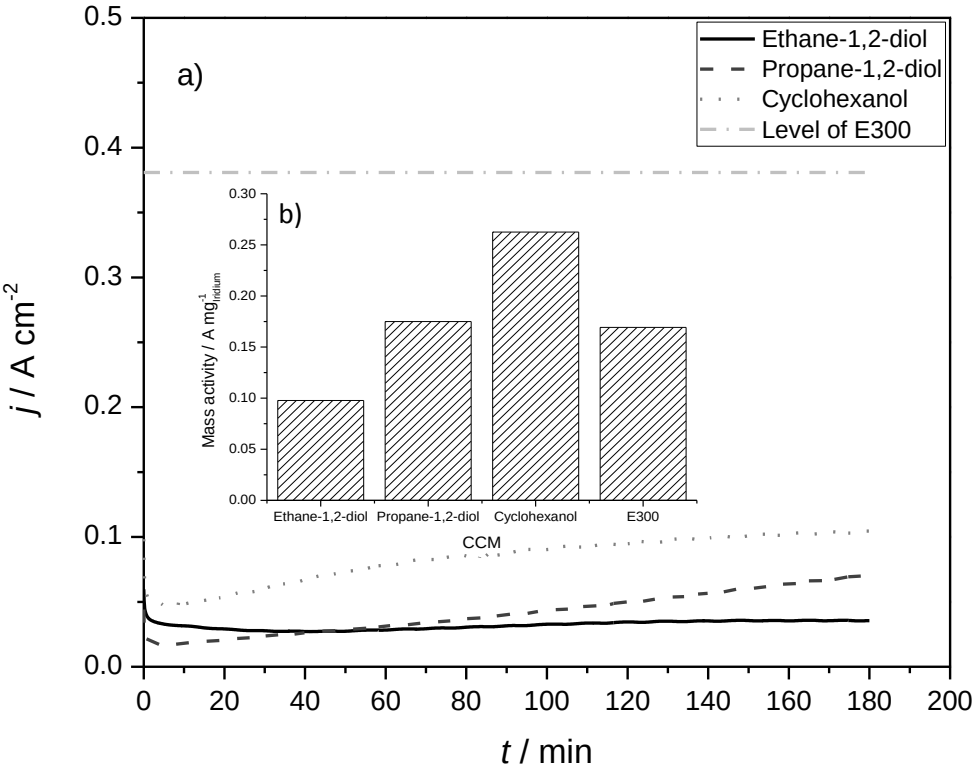

Figure 9: a) Chronoamperometries at 1.7 V and 40 ºC of CCMs with anodes coated using ethane-1,2-diol propane-1,2-diol, and cyclohexanol as solvents. b) Iridium-mass activity of fabricated CCMs and E300 (Greenerity) at 1.7 V and 40 °C.

Electrochemical impedance spectra (Figure 10) were recorded in galvanostatic mode (at 35 mA cm^{-2}) at end of tests. The EIS spectra were fitted with the equivalent circuit depicted in Figure 10 that consisted in (RQ) elements, representing a parallel combination of a resistance with a constant phase element. The high frequency resistances (R_S), associated to the electrolyte, were similar and the highest for the CCMs coated with ethane-1,2-diol and cyclohexanol (~ 0.29 Ω cm^2), the lowest for the commercial CCM (~ 0.22 Ω cm^2), followed by the CCM coated with propane-1,2-diol

(~ 0.25 Ω cm^2). R_1 is associated to the HER and the lowest values were obtained for the CCM coated with cyclohexanol and commercial CCM (~ 33 mΩ cm^2), followed by the CCM coated with ethane-1,2-diol (~ 64 mΩ cm^2) and the highest for the CCM coated with propane-1,2-diol (~ 74 mΩ cm^2). Finally, R_2 is associated to the OER and is responsible for the major contribution for the overall impedances. As discussed above and following the trend observed in the chronoamperometries (Figure 9), the values for R_2 are higher for the anodes coated with the solvents with higher relative permittivity. Among the fabricated CCMs, the highest R_2 value was obtained for the anode coated ethane-1,2-diol (~ 1.5 Ω cm^2), followed by the anode coated with propane-1,2-diol (~ 0.98 Ω cm^2) and the lowest for the anode coated with cyclohexanol (~ 0.86 Ω cm^2). Despite the commercial CCM presented the lowest R_2 among all CCMs (~ 0.56 Ω cm^2), this difference can be attributed to the higher Ir loading and to several others factors that depend on the materials and methods used in the manufacture.

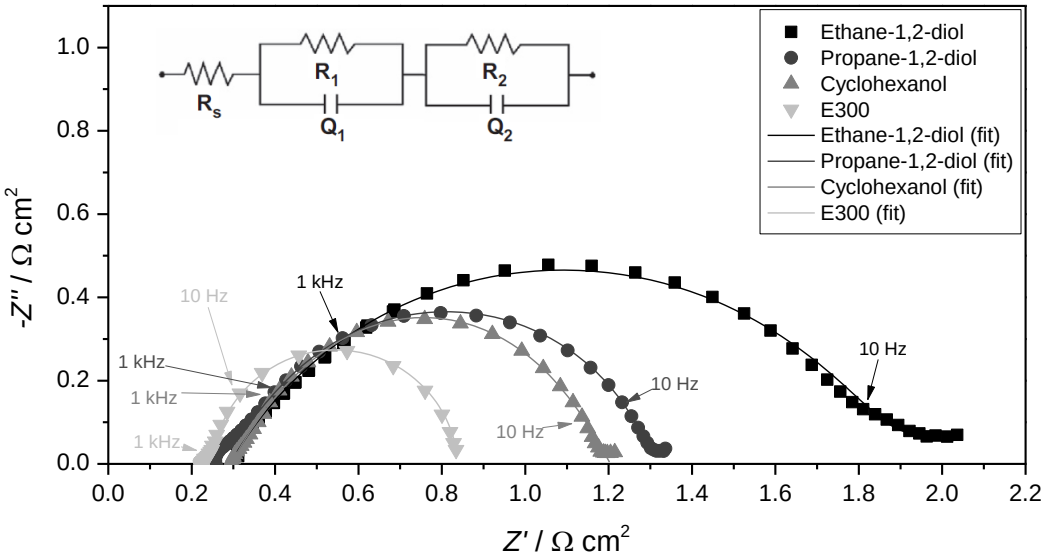

Figure 10: Impedance spectra at 35 mA cm^{-2} and 40 ºC of E300 (Greenerity) and fabricated CCMs with anodes coated using ethane-1,2-diol; propane-1,2-diol; and cyclohexanol as solvents.

CCMs	R_S / Ω	R_1 / Ω	Q_1 / F	R_2 / Ω	Q_2 / F
With swelling treatment	49.4 m	31.97 m	432.8 µ	522.6 m	579 µ
Without swelling treatment	75.76 m	51.18 m	364.3 µ	617.8 m	289.5 µ
Ethane-1,2-diol	74.1 m	16.04 m	1.482 m	374 m	998.7 µ
Propane-1,2-diol	63.37 m	18.39 m	2.345 m	244.6 m	3.945 m
Cyclohexanol	73.51 m	8.41 m	4.26 m	214.2 m	4.77 m
E300	55.31 m	8.296 m	48.73 m	146.3 m	306 m

Table 3: Parameters evaluated from EIS data fitting to equivalent circuit shown in Fig. 10 for the fabricated and commercial CCMs.

4. Conclusions

PEM electrolyzer CCMs were successfully fabricated by screen printing technique using three different solvents in the inks and a mixture of Ir-black catalyst and Ti_4O_7 support. As the electronic conductivity is correlated to the conductive surface area derived by AFM, a decrease of ionomer content could lead to a higher electrochemical performance.

This work unveils promising OER activities from inexpensive and easy-scalable screen-printed anodes with reduced iridium loadings of 0.4 ± 0.02 mg cm^{-2}, which is 83 %

lower than that of the commercial reference. The membrane swelling treatment was found to be effective, minimizing the membrane swelling during the coating process using ethane-1,2-diol as solvent of the paste, without hindering the electrolyzer performance.

Cyclohexanol was found to be a suitable single solvent for coating anodes directly on the membrane. It did not cause any noticeable swelling of the membrane thus enabling to skip the membrane swelling treatment. PEM electrolyzer tests at constant 1.7 V showed that the screen-printed CCM, using cyclohexanol as ink vehicle, delivers the highest current among all the prepared samples. The Ir-mass activity of the CCM with anode coated with cyclohexanol was 1.5 times higher than that of the commercial CCM.

Acknowledgements

The authors acknowledge the EU FP7/2007-2013 for Fuel Cell and Hydrogen Joint Technology Initiative under Grant No. 621237 (INSIDE) and to the Erasmus program of University of Porto for the financial support. The authors also acknowledge Philip Lettenmeier and Stefan Helmly for sharing their expertise regarding PEM applications; to Jorg Burkle for the assistance with wet spraying; to Oliver Freitag for the TGA measurements.

References

[1] M. Carmo, D. L. Fritz, J. Mergel, and D. Stolten, “A comprehensive review on PEM water electrolysis,” *International Journal of Hydrogen Energy*, vol. 38, no. 12. pp. 4901–4934, 2013.

[2] K. A. Friedrich, “PlanDelyKad: Study on Large Scale Water Electrolysis and

Hydrogen Storage (in German). German Federal Ministry for Economic Affairs and Energy (BMWi), Berlin," 2015.

[3] F. Barbir, "PEM electrolysis for production of hydrogen from renewable energy sources," *Sol. Energy*, vol. 78, no. 5, pp. 661–669, 2005.

[4] K. E. Ayers, C. Capuano, and E. B. Anderson, "Recent Advances in Cell Cost and Efficiency for PEM-Based Water Electrolysis," *ECS Trans.* , vol. 41, no. 10, pp. 15–22, May 2012.

[5] K. E. Ayers *et al.*, "Research Advances towards Low Cost, High Efficiency PEM Electrolysis," *ECS Trans.* , vol. 33, no. 1, pp. 3–15, Oct. 2010.

[6] L. Bertuccioli *et al.*, "Study on development of water electrolysis in the EU by E4tech Sàrl with Element Energy Ltd for the Fuel Cells and Hydrogen Joint Undertaking," Feb. 2014.

[7] U. Babic, M. Suermann, F. N. Büchi, L. Gubler, and T. J. Schmidt, "Critical Review—Identifying Critical Gaps for Polymer Electrolyte Water Electrolysis Development," *J. Electrochem. Soc.* , vol. 164, no. 4, pp. F387–F399, Jan. 2017.

[8] K. A. Lewinski, D. van der Vliet, and S. M. Luopa, "NSTF Advances for PEM Electrolysis - the Effect of Alloying on Activity of NSTF Electrolyzer Catalysts and Performance of NSTF Based PEM Electrolyzers," *ECS Trans.* , vol. 69, no. 17, pp. 893–917, Sep. 2015.

[9] S. M. Alia, S. M. Shulda, C. Ngo, S. Pylypenko, and B. S. Pivovar, "Iridium Nanowires As Highly Active, Oxygen Evolution Reaction Electrocatalysts," *Meet. Abstr.* , vol. MA2017-02, no. 37, p. 1655, Sep. 2017.

[10] P. Lettenmeier *et al.*, "Durable Membrane Electrode Assemblies for Proton

Exchange Membrane Electrolyzer Systems Operating at High Current Densities," *Electrochim. Acta*, vol. 210, pp. 502–511, Aug. 2016.

[11] B. Bladergroen, H. Su, S. Pasupathi, and V. Linkov, "Overview of Membrane Electrode Assembly Preparation Methods for Solid Polymer Electrolyte Electrolyzer," in *Electrolysis*, Dr. Janis Kleperis (Ed.), InTech, .

[12] G. Chen, S. R. Bare, and T. E. Mallouk, "Development of Supported Bifunctional Electrocatalysts for Unitized Regenerative Fuel Cells," *J. Electrochem. Soc.* , vol. 149, no. 8, pp. A1092–A1099, Aug. 2002.

[13] S. Siracusano, V. Baglio, C. D'Urso, V. Antonucci, and A. S. Aricò, "Preparation and characterization of titanium suboxides as conductive supports of IrO2 electrocatalysts for application in SPE electrolysers," *Electrochim. Acta*, vol. 54, no. 26, pp. 6292–6299, 2009.

[14] R. E. Fuentes, J. Farell, and J. W. Weidner, "Multimetallic Electrocatalysts of Pt, Ru, and Ir Supported on Anatase and Rutile TiO2 for Oxygen Evolution in an Acid Environment," *Electrochem. Solid-State Lett.* , vol. 14, no. 3, pp. E5–E7, Mar. 2011.

[15] P. Mazúr, J. Polonský, M. Paidar, and K. Bouzek, "Non-conductive TiO2 as the anode catalyst support for PEM water electrolysis," *Int. J. Hydrogen Energy*, vol. 37, no. 17, pp. 12081–12088, 2012.

[16] A. Stoyanova, G. Borisov, E. Lefterova, and E. Slavcheva, "Oxygen evolution on Ebonex-supported Pt-based binary compounds in PEM water electrolysis," *Int. J. Hydrogen Energy*, vol. 37, no. 21, pp. 16515–16521, 2012.

[17] E. Slavcheva, G. Borisov, E. Lefterova, E. Petkucheva, and I. Boshnakova,

"Ebonex supported iridium as anode catalyst for PEM water electrolysis," *Int. J. Hydrogen Energy*, vol. 40, no. 35, pp. 11356–11361, 2015.

[18] L. Wang *et al.*, "Nanostructured Ir-supported on Ti4O7 as cost effective anode for proton exchange membrane (PEM) electrolyzers," *Phys. Chem. Chem. Phys.*, vol. 18, no. 6, pp. 4487–4495, Dec. 2016.

[19] T. Ioroi and K. Yasuda, "Iridium Nanoparticles Supported on Magneli Phase Ti4O7 for PEM Water Electrolyzers," *Meet. Abstr.* , vol. MA2016-02, no. 38, p. 2419, Sep. 2016.

[20] J.-E. Won *et al.*, "PtIr/Ti4O7 as a bifunctional electrocatalyst for improved oxygen reduction and oxygen evolution reactions," *J. Catal.*, vol. 358, pp. 287–294, 2018.

[21] M. Uchida, Y. Aoyama, N. Eda, and A. Ohta, "New Preparation Method for Polymer- Electrolyte Fuel Cells," *J. Electrochem. Soc.* , vol. 142, no. 2, pp. 463–468, Feb. 1995.

[22] T. T. Ngo, T. L. Yu, and H. L. Lin, "Influence of the composition of isopropyl alcohol/water mixture solvents in catalyst ink solutions on proton exchange membrane fuel cell performance," *J. Power Sources*, vol. 225, pp. 293–303, 2013.

[23] R. Yudianti, H. Onggo, and A. Syampurwadi, "Molecular Conformation of Nafion Ionomer on Electrocatalyst Layer Prepared by Screen Printing Technique," *Int. J. Electrochem. Sci*, vol. 9, pp. 3047–3059, 2014.

[24] W. Wang, S. Chen, J. Li, and W. Wang, "Fabrication of catalyst coated membrane with screen printing method in a proton exchange membrane fuel

cell," *Int. J. Hydrogen Energy*, vol. 40, no. 13, pp. 4649–4658, 2015.

[25] C. S. Kim, Y. G. Chun, D. H. Peck, and D. R. Shin, "Method for fabricating membrane and electrode assembly for polymer electrolyte membrane fuel cells." Google Patents, 2001.

[26] E. Antolini, L. Giorgi, A. Pozio, and E. Passalacqua, "Influence of Nafion loading in the catalyst layer of gas-diffusion electrodes for PEFC," *J. Power Sources*, vol. 77, no. 2, pp. 136–142, 1999.

[27] E. Passalacqua, F. Lufrano, G. Squadrito, A. Patti, and L. Giorgi, "Nafion content in the catalyst layer of polymer electrolyte fuel cells: effects on structure and performance," *Electrochim. Acta*, vol. 46, no. 6, pp. 799–805, 2001.

[28] T. E. Springer, M. S. Wilson, and S. Gottesfeld, "Modeling and Experimental Diagnostics in Polymer Electrolyte Fuel Cells," *J. Electrochem. Soc.* , vol. 140, no. 12, pp. 3513–3526, Dec. 1993.

[29] K. Chan and M. Eikerling, "Water balance model for polymer electrolyte fuel cells with ultrathin catalyst layers," *Phys. Chem. Chem. Phys.*, vol. 16, no. 5, pp. 2106–2117, 2014.

[30] N. Agmon, "The Grotthuss mechanism," *Chem. Phys. Lett.*, vol. 244, no. 5–6, pp. 456–462, Oct. 1995.

[31] M. J. Eslamibidgoli, J. Huang, T. Kadyk, A. Malek, and M. Eikerling, "How theory and simulation can drive fuel cell electrocatalysis," *Nano Energy*, vol. 29, pp. 334–361, 2016.

[32] K.-H. Kim *et al.*, "The effects of Nafion® ionomer content in PEMFC MEAs prepared by a catalyst-coated membrane (CCM) spraying method," *Int. J.*

Hydrogen Energy, vol. 35, no. 5, pp. 2119–2126, 2010.

[33] S. Siracusano, N. Van Dijk, E. Payne-Johnson, V. Baglio, and A. S. Aricò, "Nanosized IrOx and IrRuOx electrocatalysts for the O2 evolution reaction in PEM water electrolysers," *Appl. Catal. B Environ.*, vol. 164, pp. 488–495, 2015.

[34] H.-S. Oh, H. N. Nong, T. Reier, M. Gliech, and P. Strasser, "Oxide-supported Ir nanodendrites with high activity and durability for the oxygen evolution reaction in acid PEM water electrolyzers," *Chem. Sci.*, vol. 6, no. 6, pp. 3321–3328, 2015.

[35] P. Lettenmeier *et al.*, "Nanosized IrOx-Ir Catalyst with Relevant Activity for Anodes of Proton Exchange Membrane Electrolysis Produced by a Cost-Effective Procedure," *Angew. Chemie*, vol. 128, no. 2, pp. 752–756, Jan. 2016.

[36] Z. Hou, P. Ming, D. Xing, S. Song, K. Zhang, and Y. Zhang, "Preparing method for integrated membrane-catalyst coated layer membrane electrode for a fuel cell." Google Patents, 2012.

[37] P. Lettenmeier *et al.*, "Comprehensive investigation of novel pore-graded gas diffusion layers for high-performance and cost-effective proton exchange membrane electrolyzers," *Energy Environ. Sci.*, vol. 10, no. 12, pp. 2521–2533, 2017.

[38] P. Lettenmeier *et al.*, "Low-Cost and Durable Bipolar Plates for Proton Exchange Membrane Electrolyzers," *Sci. Rep.*, vol. 7, p. 44035, Mar. 2017.

[39] P. Lettenmeier, R. Wang, R. Abouatallah, F. Burggraf, A. S. Gago, and K. A. Friedrich, "Coated Stainless Steel Bipolar Plates for Proton Exchange Membrane Electrolyzers," *J. Electrochem. Soc.*, vol. 163, no. 11, pp. F3119–F3124, Jul. 2016.

[40] A. S. Gago *et al.*, “Protective coatings on stainless steel bipolar plates for proton exchange membrane (PEM) electrolysers,” *J. Power Sources*, vol. 307, pp. 815–825, Mar. 2016.

[41] S. Siracusano, V. Baglio, F. Lufrano, P. Staiti, and A. S. Aricò, “Electrochemical characterization of a PEM water electrolyzer based on a sulfonated polysulfone membrane,” *J. Memb. Sci.*, vol. 448, no. Supplement C, pp. 209–214, 2013.

[42] C. Rozain and P. Millet, “Electrochemical characterization of Polymer Electrolyte Membrane Water Electrolysis Cells,” *Electrochim. Acta*, vol. 131, pp. 160–167, Jan. 2014.

[43] I. Dedigama *et al.*, “In situ diagnostic techniques for characterisation of polymer electrolyte membrane water electrolysers – Flow visualisation and electrochemical impedance spectroscopy,” *Int. J. Hydrogen Energy*, vol. 39, no. 9, pp. 4468–4482, Mar. 2014.

[44] K. Elsøe, L. Grahl-Madsen, G. G. Scherer, J. Hjelm, and M. B. Mogensen, “Electrochemical Characterization of a PEMEC Using Impedance Spectroscopy,” *J. Electrochem. Soc.* , vol. 164, no. 13, pp. F1419–F1426, Jan. 2017.

[45] S. Helmly, R. Hiesgen, T. Morawietz, X.-Z. Yuan, H. Wang, and K. Andreas Friedrich, “Microscopic Investigation of Platinum Deposition in PEMFC Cross-Sections Using AFM and SEM,” *J. Electrochem. Soc.* , vol. 160, no. 6, pp. F687–F697, Jan. 2013.

[46] R. Hiesgen, T. Morawietz, M. Handl, and K. A. Friedrich, “Structure and conductivity of fuel cell membranes and catalytic layers investigated by AFM,” *MRS Proc.*, vol. 1774, pp. 19–24, 2015.

[47] T. Morawietz, A. Singraber, C. Dellago, and J. Behler, “How van der Waals interactions determine the unique properties of water,” *Proc. Natl. Acad. Sci.* , vol. 113, no. 30, pp. 8368–8373, Jul. 2016.

[48] Q. Deng, C. A. Wilkie, R. B. Moore, and K. A. Mauritz, “TGA–FTi.r. investigation of the thermal degradation of Nafion® and Nafion®/[silicon oxide]-based nanocomposites,” *Polymer (Guildf).*, vol. 39, no. 24, pp. 5961–5972, 1998.

[49] G. Chen, S. R. Bare, and T. E. Mallouk, “Development of Supported Bifunctional Electrocatalysts for Unitized Regenerative Fuel Cells,” *J. Electrochem. Soc.*, vol. 149, no. 8, p. A1092, 2002.

[50] K. Senevirathne, R. Hui, S. Campbell, S. Ye, and J. Zhang, “Electrocatalytic activity and durability of Pt/NbO2 and Pt/Ti4O7 nanofibers for PEM fuel cell oxygen reduction reaction,” *Electrochim. Acta*, vol. 59, pp. 538–547, 2012.

[51] Z. Qi and A. Kaufman, “Activation of low temperature {PEM} fuel cells,” *J. Power Sources*, vol. 111, no. 1, pp. 181–184, 2002.

[52] S. Siracusano, V. Baglio, S. A. Grigoriev, L. Merlo, V. N. Fateev, and A. S. Aricò, “The influence of iridium chemical oxidation state on the performance and durability of oxygen evolution catalysts in PEM electrolysis,” *J. Power Sources*, vol. 366, no. Supplement C, pp. 105–114, 2017.